



## Plant tissue-based scaffolds filled with oil function as adipose tissue mimetics

Elyse S. Czapalay<sup>a,1</sup>, Yasamin Soleimani<sup>a,1</sup>, Jarvis A. Stobbs<sup>a,b,1</sup> ,  
Alejandro G. Marangoni<sup>a,\*</sup> 

<sup>a</sup> Dept. Food Science, University of Guelph, Guelph, ON, N1G2W1, Canada

<sup>b</sup> Canadian Light Source Inc., Saskatoon, SK, S7N 2V3, Canada

### ARTICLE INFO

**Keywords:**  
Scaffolds  
Meat analogues  
Fat  
Adipose tissue  
Oil binding  
Hardness  
Melting  
Mimetic  
Sustainability

### ABSTRACT

Cellulosic scaffolds filled with oil were designed to replicate animal adipose tissues. Many plants are structured as polysaccharide-based cellular solids. They maintain their integrity after drying, can serve as a scaffold for incorporating fat, and do not lose integrity upon heating, thus resembling native adipose tissue. Carrots, broccoli, and asparagus were freeze-dried and subsequently filled with peanut oil, its glycerolysis product (GP), and the oleogel of this GP. Oleogel-filled scaffolds displayed high oil binding capacity ( $\geq 95\%$ ), and an oil loss resembling that of adipose tissue. In addition, the texture of oleogel-filled asparagus and broccoli tissue closely resembled that of beef and pork adipose tissues, respectively. Plant scaffolds closely emulated the temperature-dependent rheological behavior of adipose tissue. These new materials could significantly improve the quality of plant-based meat analogues, such as burgers and sausages, by preventing the thermal softening of the material upon cooking and excessive oil loss.

### 1. Introduction

Population growth across the globe has led to increased demand for meat and meat products. Meeting this increased demand could put a serious strain on the environment due to greenhouse gas emissions, deforestation, excessive use of freshwater resources, and loss of biodiversity associated with meat production (Poore and Nemecek, 2018). Plant-based meat analogues offer a more environmentally friendly solution to the increased demand for meat worldwide (Palomo-Vélez et al., 2018). One problem is that consumers anticipate plant-based alternatives to match the flavour, texture, nutritional profile, and appearance of their animal-derived counterparts (Craig et al., 2022). The focus in plant-based meat analogues has been on plant protein functionality, using extrusion and 3D printing methods. Meanwhile, the other components of animal meat, such as pigments, colour, and fat, have not received as much attention.

Unstructured plant fats and oils, such as coconut oil, are most often used in place of adipose tissue (Soleimani et al., 2023). However, adipose tissue provides important characteristics such as juiciness,

chewiness, and hardness to meat, that coconut oil, or other oils, cannot. Therefore, attention must be shifted towards creating an equivalent to adipose tissue to optimize plant-based meat analogues.

In recent years there have been more studies that attempt to create adipose tissue mimetics but there are still many challenges. Many of these studies utilize oleogels and emulsion gels to create adipose tissue mimetics. Oleogels and emulsion gels fall short of mimicking animal adipose tissue in terms of the resilience of the gels upon cooking. Most oleogels and emulsion gels soften upon heating, lose oil, and thus lose all functionality (Czapalay and Marangoni, 2024). For an adipose tissue mimetic to adequately resemble adipose tissue, thermal resilience must be improved. Although fat inside animal adipose tissue becomes molten at cooking temperatures, the tissue can maintain, or even gain strength. Rheological strain and frequency sweeps of pork, lamb, and beef adipose tissue before heating (20 °C), 80 °C, and cooling back to 20 °C show that even at cooking temperatures, animal adipose tissue remains solid (Wijarnprecha et al., 2022a). Currently, there are no plant-based strategies that fulfill this requirement.

Adipose tissue is composed of a collagen network filled with

This article is part of a special issue entitled: The Green Transition published in Current Research in Food Science.

\* Corresponding author.

E-mail address: [amarango@uoguelph.ca](mailto:amarango@uoguelph.ca) (A.G. Marangoni).

<sup>1</sup> . Equal contributions.

<https://doi.org/10.1016/j.crf.2025.101002>

Received 17 December 2024; Received in revised form 7 February 2025; Accepted 9 February 2025

Available online 12 February 2025

2665-9271/© 2025 The Authors. Published by Elsevier B.V. This is an open access article under the CC BY-NC-ND license (<http://creativecommons.org/licenses/by-nc-nd/4.0/>).

adipocytes containing fat. This network allows for oil to be retained after cooking and is responsible for textural properties such as hardness and chewiness being maintained. He et al. (2021) discuss the natural supporting structures, or scaffolds, present in plant tissue, and how they could be beneficial in creating more realistic plant-based meat products. Another study used apple scaffolds to mimic certain properties and help regenerate adipose tissue in humans (Contessi Negrini et al., 2020). The microstructural similarities between the collagen network in animal adipose tissue and some plant scaffolds (especially celery and carrot) are remarkable and led to the hypothesis that vegetable scaffolds could provide an appropriate scaffold that could be filled with fats and oils and function as an adipose tissue mimetic (Contessi Negrini et al., 2020; Wijarnprecha et al., 2022b).

In addition to the microstructure of plant scaffolds, it is important to consider what type of oil is being used to fill them. Unsaturated oils and oils with specific wetting abilities are desired to penetrate the pore structure of the scaffold efficiently. Recently, we reported on a novel strategy to convert liquid oils into solid fats using enzymatic glycerolysis (Soleimani et al., 2023). Glycerolized oils offer solidity regardless of their low saturated fat content. Moreover, they are quite surface active due to their high content of partial glycerides (30–35% monoacylglycerols, 45–50% diacylglycerols, and 15–20% triacylglycerols). This surface activity may aid in the incorporation of the oil into the dry cellular structure.

Here we show how freeze-dried plant tissue filled with peanut oil, the glycerolysis product (GP) of peanut oil, and oleogels of this GP can mimic the thermal and mechanical properties of pork and beef adipose tissue, as indicated by texture profile analysis, small-deformation rheology, oil loss measurements, and synchrotron micro-computed tomography. Such natural adipose tissue mimetics would allow for the manufacturing of plant-based meat analogues that more closely resemble their animal counterparts. An increase in the consumption of plant-based meat products would lead to an increase in the sustainability of our food supply by decreasing pressure on land use, the need for deforestation, and freshwater use.

## 2. Materials and methods

### 2.1. Materials

Various vegetables, peanut oil, and raw meat materials were purchased from a local market (Guelph, ON, Canada) and their visible adipose tissues (intermuscular fat) separated and used for the experiments. Glycerol (99.7% USP grade, Ingredient Depot) was purchased online. Candida antarctica lipase B immobilized on Immobead 150 was purchased from Sigma-Aldrich (Sigma-Aldrich; St. Louis, MO, USA). Ethylcellulose powder with viscosity of 45 cP (EC45) was obtained from Dow company.

### 2.2. Glycerolysis reaction

Peanut oil was enzymatically modified using the nonregiospecific Candida antarctica lipase B, immobilized on Immobead 150, added at 2 wt% relative to the oil. Reactions were conducted with 1:1 oil to glycerol molar ratio, at 65 °C, and under continuous agitation (100 rpm) for 72 h (Soleimani et al., 2023).

### 2.3. Oleogel preparation

GP-oleogel was formulated by combining glycerolized peanut oil with EC at a 5% w/w concentration described in our previous work (Soleimani et al., 2024b).

### 2.4. Oil filled scaffolds

Slices of carrot and broccoli stem (5 mm thick, 20 mm in diameter),

as well as asparagus slices (5 mm thick, using the natural diameter of the asparagus), were cut with a mandolin slicer and freeze-dried at –50 °C and a pressure of 0.05 mBar (Labconco FreeZone 2.5L Benchtop Freeze Dryer). These dried plant scaffolds were filled with different oil systems, such as peanut oil, glycerolized peanut oil (GP), and its EC oleogel.

Oil absorption was performed by immersing of dried samples in pre-heated oils and incubating for 30 min at 50–60 °C to facilitate oil penetration. The ratio of sample to oil was 1:10 (w/w). Samples were then removed from oil and weighed after gentle swabbing to remove excess oil from the surface. Oil absorption capacity (g/g) was measured gravimetrically using a (balance model) analytical balance with a precision of 0.1 mg. Plant derived scaffolds were then stored at 5 °C for a minimum of two days before subsequent analysis to ensure oil stabilization and crystallization.

Oil binding capacity (OBC) was studied by measuring the oil release during heating. The sample was heated for 30 min at 60 °C, and the released oil was collected by placing the sample on pre-weighed filter paper. After cooling, the filter paper with absorbed oil was weighed again to determine the amount of oil released. OBC was calculated using the following formula:

$$\text{OBC (\%)} = \frac{\text{Initial oil weight} - \text{Oil released}}{\text{Initial oil weight}} \times 100$$

### 2.5. Texture analysis

A TA-XT2 texture analyzer (Stable Micro Systems Ltd., Texture Technologies Corp., Scarsdale, NY, USA) with the Texture Exponent software was used to determine texture properties of oil filled scaffolds in comparison to adipose tissue. A parallel plate double compression test was performed with a 3-inch diameter aluminum plate 30 kg load cell, using a test speed of 1 mm/s and a 5 s interval between the two compression cycles. Specimens were deformed using a 50% strain. For adipose tissue, to ensure conformity with the shape and dimensions of the plant scaffolds, cylindrical sections measuring 20 mm in diameter and 5 mm in height were excised from fresh tissues. These adipose samples were subsequently stored in a refrigerator at 5 °C for at least two days before the analysis was carried out. Parameters such as hardness, gumminess, springiness, cohesiveness, and chewiness were extracted from the resulting curves. All measurements were conducted in triplicate.

### 2.6. Temperature sweep

Oscillatory temperature sweeps were conducted using a rotational rheometer (MRC 302, Anton Paar, Graz, Austria) equipped with a 20 mm parallel plate geometry (PP20). A gap was set to 1 N. Cylindrical sections of adipose tissue, carrot, and broccoli plant scaffolds (20 mm in diameter, 2.5 mm in height), along with asparagus slices (natural diameter of the asparagus, 2.5 mm in height), were used for the experiments. To prevent slippage during plant scaffold analysis, the top and bottom plates were affixed with sandpaper. The temperature-dependence of samples was measured using the following protocol: (i) an isothermal hold at 5 °C for 10 min (ii) heating from 10 to 100 °C at rate of 5 °C/min, under a constant strain of 0.1% and frequency of 1 Hz. All samples were analyzed in triplicate. A normal force of 0.5 N was applied during the measurements of adipose tissue to ensure continuous contact between the plates and the sample.

### 2.7. Synchrotron-based microcomputed tomography (SR- $\mu$ CT) phase contrast imaging (PCI)

Synchrotron-based microcomputed tomography phase contrast imaging (SR- $\mu$ CT PCI) was performed at the Biomedical Imaging and Therapy Bending Magnet beamline (BMIT-BM 05B1-1) at the Canadian Light Source Synchrotron (CLS). Data were collected similarly to those

previously described in Chen et al. (2021) and Stobbs et al. (2024). Plant scaffolds were cut into  $\sim 5 \times 5 \times 3$  mm cubes and mounted in a custom sample nest holder 3D printed at the CLS. This was subsequently mounted on a Huber manual goniometer stage for data collection. A PCO Edge 5.5 sCMOS camera ( $2160 \times 2560$  pixels) coupled with an Optique Peter (Lentily)  $5 \times$  objective (Mitutoyo LWD Plan Apochromate) and  $0.9 \times$  eyepiece microscope gave an effective pixel size of  $1.44 \mu\text{m}$  and FOV of  $3.70 \text{ mm H} \times 3.12 \text{ mm W}$ . A  $50 \mu\text{m}$  thick Lutetium Aluminum Garnet: Cerium (LuAG:Ce) scintillator (European Synchrotron Radiation Facility) was used. The combination of camera, optics and scintillator are collectively known as the “detector-setup”. For rapid scanning of samples an Aluminum (0.8 mm) + Silver (0.100 mm) filtered white beam was used. A single  $\mu\text{CT}$  scan consisted of 10 flat images (beam on detector with no sample), 10 dark images (no beam on detector), and 2000 projection images (sample in beam path). The flat and dark images are used to remove system noise and normalize projection images for reconstructions. The sample was placed 4 cm from detector also known as the sample-to-detector distance (SDD).

Image processing and three-dimensional reconstructions were done similar to those described by Willick et al. 2020 and Stobbs et al. (2024). Data were reconstructed using the TOFU software described by Vogelgesang et al. using the Paganin phase-retrieval method (Faragó et al., 2022; Paganin et al., 2002). A 4 cm sample SDD, beam energy of 25.5 keV, and  $\delta/\beta$  of 150 were used. A large spots filter and ring removal algorithm were used to remove to suppress image artifacts. 32-bit images were cropped and converted to 8-bit images before being saved as final tiff image stacks. Reconstructed slices were cropped to  $1600 \times 1600 \times 1550$  pixels which results in  $2.3 \text{ mm} \times 2.3 \text{ mm} \times 2.2 \text{ mm}$  volumes for analysis. Final image stacks were opened, visualized, and segmented in 3D data visualization software Avizo 2020.2 (Thermo Scientific Amira-Avizo Software, Thermo Fisher Scientific, Waltham, MA USA). 8-bit histograms were produced in Avizo by using the bit depth range between 0 and 255 with a bin width of 1 producing 256 bins. CT histogram [count of volume pixels (voxels) vs grey-value in 8-bit of the entire CT volume] was deconvoluted by manual selection to

identify the contributions of each region of interest, i.e., air filled pores, oil-filled pores, oil, and plant scaffold from a single slice and plotted against the entire CT histogram and can be seen in the  $\mu\text{CT}$  analysis summary video in the third figure. Samples were manually segmented in Avizo for porosity, pores size analysis before oil filling and volume fraction of oil filling. An example segmentation and analysis process can be seen in the summary  $\mu\text{CT}$  analysis video in the second figure. Excel was used for final analysis, calculations and plotting.

## 2.8. Statistical analysis

All analyses were performed in triplicate. Statistical analysis for all data was conducted using GraphPad Prism 10.3.1. One-way ANOVA and Tukey’s Multiple Comparison Test were used to assess significance between samples at  $P < 0.05$ .

## 3. Results and discussion

### 3.1. Oil absorption and loss

High oil absorption and OBC are essential characteristics for these systems, especially as their structure may be disrupted during incorporation into a food product. Freeze-dried asparagus exhibited the highest oil absorption capacity-up to five times its initial weight (Fig. 1A). Additionally, plant scaffolds demonstrated a high oil retention capacity, within the range of 80–90 % (w/w), when filled with GP, and as much as 95% (w/w) when filled with oleogel (Fig. 1B).

Supplementary Figure 1 shows oil loss from various plant scaffolds filled with different oil systems, as well as from beef and pork adipose tissues, after heating. The oil stains on the filter paper reflect the extent of oil release, demonstrating differences in OBC under thermal conditions. Beef and pork adipose tissues exhibited approximately 10 % and 20 % oil loss, respectively. The asparagus scaffolds had the overall best ability to retain oil (Fig. 1B) such that even the oil-filled asparagus scaffold had lower oil loss than GP or oleogel-filled broccoli and carrot

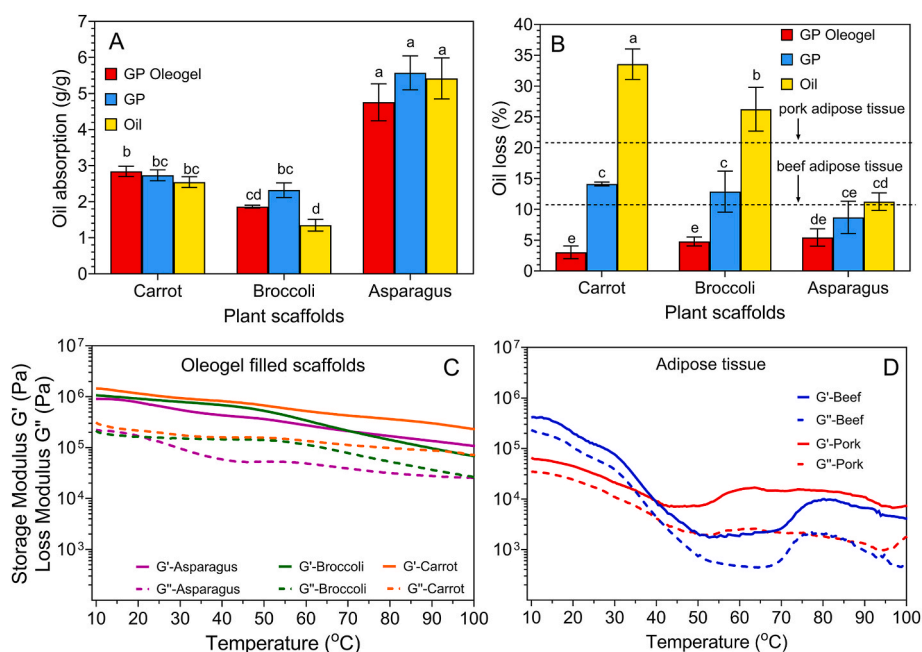


**Fig. 1.** Oil absorption, oil loss, and thermal rheology of plant scaffolds filled with different oil systems. (A) Oil absorption (g oil/g scaffold) for three plant scaffolds (S1, S2, S3) filled with three different oil systems (O1:Oleogel, O2:Glycerolysed oil, O3: native oil). (B) Oil loss (%) for the same scaffolds and oil systems after incubation at  $60^\circ\text{C}$ , 1 h. The dashed lines represent the mean oil loss for pork and beef adipose tissue without statistical comparison to the plant scaffold samples. (C) Small-deformation dynamic rheological thermal profiles of plant scaffolds filled with GP-oleogel, (D) Small-deformation dynamic rheological thermal profiles of beef and pork adipose tissue. The labelled numbers in (C) and (D) correspond to the  $G'$  and  $G''$  values at 10 and  $80^\circ\text{C}$ . Values in (A) and (B) are mean ( $n = 3$ )  $\pm$  standard deviation. Values followed by different superscript letters (a–e) are statistically different ( $P < 0.05$ ).

scaffolds ( $P < 0.05$ ). Moreover, scaffolds filled with unstructured oil displayed the highest oil release, while those containing oleogel and GP displayed greater oil retention (Fig. 1B). This demonstrates the unique ability that GP possesses to provide structure to unsaturated oils. The scaffolds filled with unstructured oil experienced minor oil loss just after oil absorption while the GP-oleogel filled scaffolds did not experience any oil loss prior to heating. Oil loss from scaffolds containing GP was lower than of the original oil, while oleogels of this GP displayed an even lower oil loss.

Achieving a more porous structure with larger pore sizes, along with minimizing structural damage during drying, could lead to higher oil absorption. Therefore, it is important to continue investigating other plant tissues to use as scaffolds, such as apple scaffolds which have larger pores than carrot scaffolds (Contessi Negrini et al., 2020). In addition, the composition of the oil can also influence OBC. Our results show that the physical state of oil (liquid/solid) at different temperatures, and its polarity are associated with OBC.

### 3.2. Texture profile analysis

Adipose tissue plays an important role in the texture of meat, such as hardness, chewiness, and a fatty sensation. Comparing animal adipose tissue to an adipose tissue mimetic is critical to understanding how the mimetic will behave in a plant-based meat analogue. Table 1 presents the texture profile analysis of GP-oleogel, GP, and oil-filled plant scaffolds with statistical comparison to pork and beef adipose tissue.

The hardness of pork adipose tissue ( $59.82 \pm 9.48$  N) is about 1.9 times less than beef adipose tissue ( $115.96 \pm 8.15$  N). The filled scaffolds shown in Table 1 had a range of hardness values where some scaffolds could replicate the firmer beef adipose tissue and others were a closer match to the hardness of softer pork adipose tissue. However, oil-filled broccoli scaffolds were softer than both pork and beef adipose tissues. Carrot scaffolds, on the other hand, were harder than even beef adipose tissue. The carrot scaffolds did not match the cohesiveness of either beef or pork. GP-oleogel and GP filled asparagus scaffold samples also had lower cohesiveness than the pork and beef adipose tissue values. Although the carrot scaffold samples had hardness and cohesiveness values that were not ideal, their gumminess values were able to match both beef and pork adipose tissue. The only other sample that achieved similar gumminess was GP-filled asparagus which had similar gumminess to pork adipose tissue. The springiness values of all scaffold samples mirrored the springiness values of pork and beef adipose tissue ( $P < 0.05$ ). Only two of the nine scaffold samples lacked chewiness, GP-oleogel asparagus and GP broccoli. The oil filled broccoli scaffold had similar chewiness to pork adipose tissue while the remaining samples were able to match the chewiness of both pork and beef adipose tissue ( $P < 0.05$ ).

**Table 1**

Texture profile analysis results for the scaffold-oil systems compared to beef and pork adipose tissues.

Oil-filled scaffolds	Hardness (N)	Springiness (mm)	Cohesiveness (–)	Gumminess (N)	Chewiness (N)
<b>Carrot</b>					
GP-Oleogel	167.77 $\pm$ 12.71 <sup>a</sup>	0.40 $\pm$ 0.10 <sup>a</sup>	0.12 $\pm$ 0.01 <sup>de</sup>	19.67 $\pm$ 3.80 <sup>abc</sup>	7.61 $\pm$ 0.68 <sup>abcd</sup>
GP	175.78 $\pm$ 9.41 <sup>a</sup>	0.37 $\pm$ 0.06 <sup>a</sup>	0.15 $\pm$ 0.02 <sup>de</sup>	25.91 $\pm$ 4.76 <sup>a</sup>	10.32 $\pm$ 3.26 <sup>a</sup>
Oil	162.28 $\pm$ 25.92 <sup>a</sup>	0.23 $\pm$ 0.03 <sup>a</sup>	0.13 $\pm$ 0.05 <sup>de</sup>	21.94 $\pm$ 11.34 <sup>ab</sup>	4.79 $\pm$ 1.89 <sup>ae</sup>
<b>Asparagus</b>					
GP-Oleogel	99.34 $\pm$ 4.66 <sup>bc</sup>	0.36 $\pm$ 0.07 <sup>a</sup>	0.08 $\pm$ 0.03 <sup>e</sup>	8.08 $\pm$ 2.26 <sup>cd</sup>	3.01 $\pm$ 1.28 <sup>de</sup>
GP	71.22 $\pm$ 5.26 <sup>cd</sup>	0.50 $\pm$ 0.03 <sup>a</sup>	0.13 $\pm$ 0.03 <sup>de</sup>	9.53 $\pm$ 2.98 <sup>bd</sup>	4.76 $\pm$ 1.45 <sup>ae</sup>
Oil	28.79 $\pm$ 6.57 <sup>ef</sup>	1.29 $\pm$ 1.22 <sup>a</sup>	0.23 $\pm$ 0.03 <sup>bcd</sup>	6.50 $\pm$ 0.73 <sup>d</sup>	3.68 $\pm$ 0.12 <sup>be</sup>
<b>Broccoli</b>					
GP-Oleogel	53.10 $\pm$ 4.17 <sup>de</sup>	0.53 $\pm$ 0.01 <sup>a</sup>	0.20 $\pm$ 0.05 <sup>bcd</sup>	10.54 $\pm$ 2.71 <sup>bd</sup>	5.62 $\pm$ 1.52 <sup>ae</sup>
GP	34.17 $\pm$ 11.78 <sup>ef</sup>	0.40 $\pm$ 0.01 <sup>a</sup>	0.16 $\pm$ 0.02 <sup>ce</sup>	4.47 $\pm$ 2.68 <sup>d</sup>	1.81 $\pm$ 1.12 <sup>e</sup>
Oil	19.97 $\pm$ 2.4 <sup>f</sup>	0.58 $\pm$ 0.01 <sup>a</sup>	0.31 $\pm$ 0.04 <sup>ab</sup>	6.07 $\pm$ 0.87 <sup>d</sup>	3.52 $\pm$ 0.53 <sup>ce</sup>
<b>Adipose tissue</b>					
Beef	115.96 $\pm$ 8.15 <sup>b</sup>	0.29 $\pm$ 0.00 <sup>a</sup>	0.26 $\pm$ 0.01 <sup>ac</sup>	30.49 $\pm$ 2.75 <sup>a</sup>	8.91 $\pm$ 0.82 <sup>ab</sup>
Pork	59.82 $\pm$ 9.48 <sup>de</sup>	0.37 $\pm$ 0.12 <sup>a</sup>	0.37 $\pm$ 0.08 <sup>a</sup>	21.63 $\pm$ 4.39 <sup>ab</sup>	8.05 $\pm$ 2.61 <sup>abc</sup>

Values are mean ( $n = 3$ )  $\pm$  standard deviation. Values followed by different superscript letters (a-e) within the same column are statistically different ( $P < 0.05$ ).

GP and GP-oleogel filled scaffolds were harder than their native oil-filled counterparts for each vegetable scaffold. Since lack of firmness is a common theme observed in adipose tissue mimetics, this further demonstrates the benefits of using GP in adipose mimetic formulations.

Of all the filled scaffold combinations, the asparagus scaffold filled with GP was able to most closely mimic the textural properties of an adipose tissue, specifically pork adipose tissue. GP-filled asparagus scaffold matched the hardness, springiness, gumminess, and chewiness of pork adipose tissue. This sample did not match the cohesiveness of pork adipose tissue however, the cohesiveness was similar to that of beef adipose tissue ( $P < 0.05$ ).

### 3.3. Thermal rheology

It is known that adipose tissue maintains its form during heating and helps prevent the trapped oil from leaking out once molten. When unstructured plant fats/oils, such as coconut oil, are incorporated into plant-based meat analogues, they melt upon cooking and thus lose their solid structure. To understand whether the filled scaffolds are good adipose tissue mimetics, it is important to characterize their thermal behaviour.

To observe the general softening behavior during cooking, we examined the temperature-dependent changes in the oil filled scaffolds and pork and beef adipose tissue (Fig. 1C and D and Supplementary Figure 2). The plant scaffolds showed a consistent, gradual decline in elastic modulus ( $G'$ ) and loss modulus ( $G''$ ) during heating, which can be attributed to the melting of fat crystals in the oleogel and GP incorporated scaffolds, as well as the softening of the plant tissue at higher temperatures (Fig. 1C and Supplementary Figure 2). Adipose tissue samples exhibited a complex thermal behavior, with a pronounced softening and decline in both  $G'$  and  $G''$  by heating from 10 to  $\sim 50$  °C. Upon heating from 50 °C to 80 °C, the  $G'$  and  $G''$  values increased substantially while the predominant elastic nature ( $G' > G''$ ) was retained at the entire temperature range (10–90 °C) (Fig. 1D). This behaviour is caused by the denaturation of protein that occurs at elevated temperature and the resulting tightening of the collagen network (Soleimanian et al., 2024a).

Interestingly, scaffolds and adipose tissues exhibited similar stiffness, indicated by their  $G'$  values. At 10 °C, the  $G'$  values for broccoli, asparagus, and beef adipose tissue were within the same order of magnitude, ranging between 100 and 1000 KPa. This suggests a comparable level of structural rigidity and resistance to deformation, indicating that the elastic properties of the scaffolds effectively mimic those of adipose tissue. Carrot showed slightly greater  $G'$  versus other scaffolds and lower stiffness was found in pork adipose tissue compared to beef. The lower stiffness of pork adipose tissue versus beef agrees with the hardness results determined by texture profile analysis. Like adipose tissue, the

elastic response of the plant scaffolds was maintained during heating, highlighting the ability of plant scaffolds to replicate the mechanical behavior of adipose tissue with temperature. There are currently no systems that can achieve this since most soften excessively.

These findings demonstrate the potential use of plant scaffolds as adipose tissue mimetics in food applications where texture and firmness are crucial.

### 3.4. Synchrotron-Based Microcomputed Tomography phase contrast imaging

Synchrotron-Based Microcomputed Tomography (SR- $\mu$ CT) Phase Contrast Imaging (PCI) was used to investigate the microstructure of plant scaffolds before and after oil filling. SR- $\mu$ CT enables rapid and non-destructive three-dimensional imaging of a sample. By using phase retrieval methods during image reconstruction, a boost to the signal-to-noise ratio will increase the contrast of the resulting images, enabling easier segmentation and interpretation of images. Using this technique, it was possible to distinguish oil absorbed in the scaffold pores and into the scaffold material separately. The summary “ $\mu$ CT analysis movie” showing detailed steps in the analysis is available in the supplementary materials. Fig. 2 shows the scaffolds before and after oil filling using this technique.

All scaffolds had a total porosity of about 90% before oil filling (Table 2). However, the scaffolds exhibited a significant visual difference in pore size and shape, as shown in Figs. 2 and 3.

The asparagus scaffold had significantly smaller and more numerous pores contrary to broccoli and carrot scaffolds (Fig. 3). Slide 9 of the  $\mu$ CT analysis movie and SF4 demonstrates that asparagus scaffolds had a higher pore count (1964 total pores) than carrot (1177) and broccoli (366) scaffolds, additionally it shows that the asparagus scaffold had a more heterogenous range of shape and size of its pores. Fig. 3 demonstrates that the carrot scaffold contained large, elongated pores, while the broccoli scaffold had highly interconnected pores. The interconnected pores in the broccoli scaffold are shown in Fig. 3, where one single large red pore is visible.

The interconnected pores of broccoli could explain why a higher percentage of pores were filled in broccoli compared to asparagus and carrot (Table 2). In the broccoli, the scaffold itself absorbed less oil than in carrot and asparagus samples. This is likely because the larger pore size meant that upon filling less oil would be directly exposed to the

**Table 2**

Volume fraction analysis from synchrotron-based microcomputed tomography phase contrast imaging of scaffold systems before and after peanut oil absorption.

	Asparagus	Broccoli	Carrot
Segmentation	Volume Fraction		
<i>Before Oil Absorption</i>			
Scaffold	9.97%	8.64%	8.35%
Pore (air)	90.03%	91.36%	91.65%
<i>After Oil Absorption</i>			
Scaffold	16.89%	9.52%	16.89%
Pore (air)	38.95%	10.14%	38.95%
Pore (oil)	44.16%	80.35%	44.02%
Percent pores filled	53.13%	88.80%	53.05%
Oil in Scaffold	6.92%	0.88%	8.54%

walls. Fig. 2D–F illustrate the absorption and permeation of oil into these scaffolds, highlighting the variations in how each structure interacts with and retains oil. The filled scaffolds in Fig. 3 and Supplementary Figure 3 resemble images of pork adipose tissue reported in previous work (Wijarnprecha et al., 2022b). The asparagus scaffold had oil droplets in the scaffold with diameters roughly equal to the adipocytes of pork adipose tissue (about 200  $\mu$ m).

A histogram shows a volumetric density distribution where lower values indicate a relatively lesser dense material than higher values. By plotting the total voxels (volume pixels) of an image stack vs grey value we can identify several peaks for each sample (Supplementary Slide 5). These peaks arise from each component (air, oil and scaffold) in a CT scan. Much like the visual image analysis we can use a histogram to see relative changes in a volume. We can see in Supplementary Slide 6 the scaffolds with no oil (red line), peaks which are being formed by the volume of air (50–100) and scaffold (150–200). A unique feature of phase retrieved images is the phase effect which manifests as light and black fringes on the interface of two different materials (i.e. air and organic material). The result of which can be used to look at relative changes in the size and number of pores or particles (Sivakumar et al.).

When an air peak widens the relative size distribution increases and inversely, when a peak sharpens there is a smaller size distribution. It can be observed that there are two air peaks in the non-oil filled scaffold. Of these two peaks there is one sharp peak due to small pores within the scaffold which we can refer to as intra-scaffold pores and a broad peak

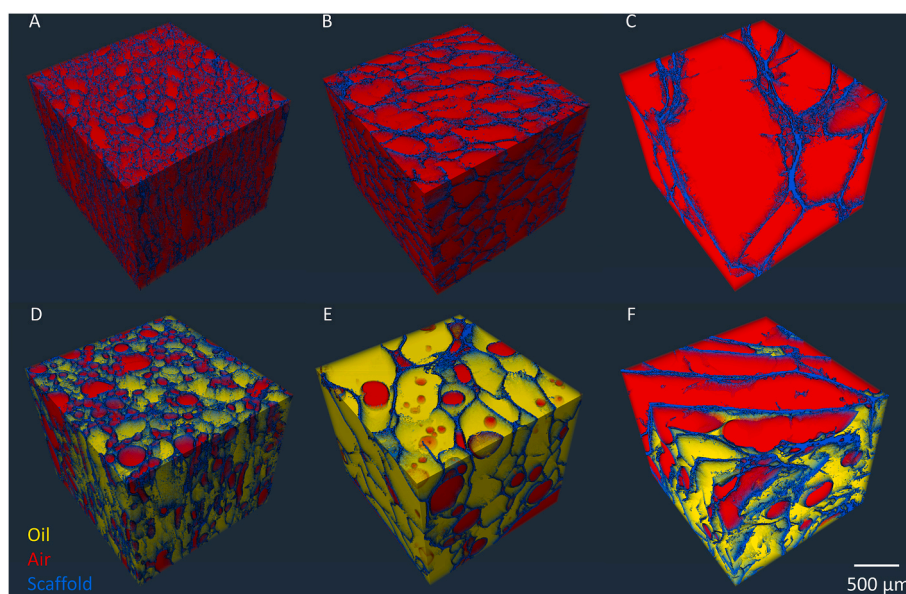


**Fig. 2.** Synchrotron-based microcomputed tomography phase contrast imaging volume rendered segmentations of unfilled scaffolds, (A) asparagus, (B) broccoli, (C) carrot, and oil-filled scaffolds of (D) asparagus, (E) broccoli, and (F) carrot. Red represents air, blue plant scaffold, and yellow represents oil.

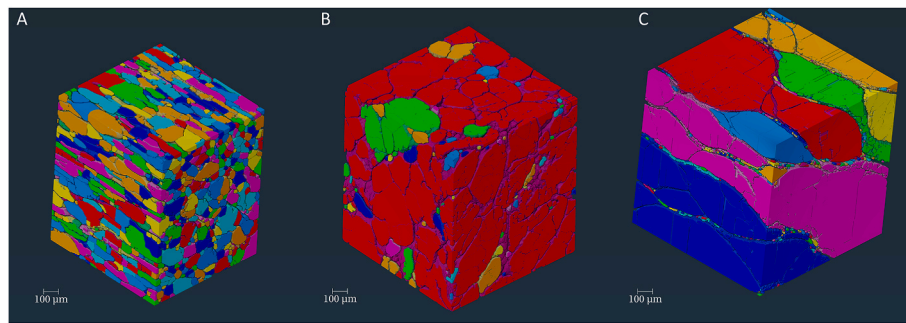


**Fig. 3.** Synchrotron-based microcomputed tomography phase contrast imaging volume rendering of air pore analysis showing differences of pore size and structure between A) asparagus, B) broccoli, and C) carrot.

arising from a large size range of pores in the inter regions of pores, which we can refer to as inter-scaffold pores. The large wide peak between  $\sim 140$  and  $200$  arises from large thickness variations of the scaffold wall material as well as relative differences in scaffold density. By comparing the relative changes in peak width and grey-value in the histogram we can conclude that asparagus scaffold has a smaller scaffold wall thickness and smaller wall thickness variations of the scaffolds and the carrot has the largest variation of wall thickness which is confirmed when visually observing the reconstruction CT slices.

After oil filling a new peak arises in all scaffolds at  $\sim 110$  8-bit grey-values. This sharp peak is from liquid oil which has a homogenous density and thus sharper peak in all histograms. There is a second broad peak which arises around  $\sim 150$  8-bit grey-values in all scaffolds after oil filling. This peak is oil-absorbed in the intra-scaffold pores and scaffold material and manifests a lower grey-values as the oil-absorbed material is less dense than non-oil absorbed scaffold material. This also suggests as the number of voxels of non-oil absorbed scaffold material is reducing in number as seen in Supplementary Slide 5. This is observed in all asparagus, broccoli, and carrot scaffolds histograms.

It is important to note the reduction in the scaffold peak due to oil absorption into the tissue is beyond the spatial resolution ( $\sim 4.3 \mu\text{m}$ ) of the detector set-up and this phenomenon is only observable through lowering of grey values in oil absorbed material. We can therefore conclude from the histogram analysis the increase in scaffold volume fraction after oil filling is due to oil absorption into, and expansion of, the scaffold. This may cause higher retention of oil when compressed. As a result, asparagus and carrot scaffold may have a gummier, less brittle, texture compared to broccoli due to the oil absorbed into the scaffold (recall Table 1).

While it is interesting that these plant scaffolds visually resemble adipose tissue, they also have similar structural features. Asparagus, broccoli, and carrot scaffolds are all about 10% scaffold and 90% pore (Table 2) while adipose tissue can contain up to 80% fat (Wijarnprecha et al., 2022b). The 90% pore value represents how much oil can be absorbed into the scaffolds. Supplementary Movies 1-6 offer a 360° view of the three vegetable scaffolds before and after oil absorption and further shows the similarities between the oil pockets in the scaffold matrix and adipocytes. Movie 5 displays the homogenous oil distribution in filled broccoli scaffolds. This agrees with the data in Table 2 which shows that the pores of broccoli scaffolds were almost entirely filled. Broccoli scaffold pores were 88.80% filled after oil absorption while asparagus and carrot scaffold pores were both around 53% filled (Table 2). However, this is not to say that the asparagus and carrot lost the oil rather than the oil was absorbed into the scaffold walls instead of the pores.

#### 4. Conclusion

Oil-filled freeze-dried plant tissue had comparable mechanical, rheological and oil binding properties to pork and beef adipose tissue.

The plant tissue scaffolds offered a plant-based alternative for achieving the functionality and structural integrity required for meat analogues, providing new opportunities for the development of sustainable, texture-optimized meat substitutes. The oil binding capacity and mechanical properties appear to be influenced by the composition of the support material and structural changes during drying. Moving forward, investigating more plant tissue scaffolds with different pore sizes, pore shapes and mechanical characteristics would lead to further optimization. Moreover, the potential is there to use these plant tissue-based scaffolds for cellular meat production and any application where a more natural and inexpensive scaffold is required to create structure. Overall, plant scaffolds offer a unique and effective way to create adipose tissue mimetics that will help improve plant-based meat analogues, and in turn help improve the sustainability of the global food supply.

#### CRediT authorship contribution statement

**Elyse S. Czupalay:** Investigation, Validation, Data curation, Writing – original draft, Visualization. **Yasamin Soleimani:** Methodology, Validation, Formal analysis, Data curation, Writing – review & editing, Visualization. **Jarvis A. Stobbs:** Methodology, Software, Validation, Formal analysis, Data curation, Writing – review & editing, Visualization. **Alejandro G. Marangoni:** Conceptualization, Methodology, Validation, Resources, Data curation, Writing – review & editing, Supervision, Project administration, Funding acquisition.

#### Declaration of competing interest

The authors declare that they have no known competing financial interests or personal relationships that could have appeared to influence the work reported in this paper.

#### Acknowledgments

Part of the research described in this paper was performed at the Canadian Light Source, a national research facility of the University of Saskatchewan, which is supported by the Canada Foundation for Innovation (CFI), the Natural Sciences and Engineering Research Council (NSERC), the National Research Council (NRC), the Canadian Institutes of Health Research (CIHR), the Government of Saskatchewan, and the University of Saskatchewan. CT data handling, processing, and analysis on this paper was partially supported by the grant and contribution-funding program of the National Research Council of Canada. J.A.S. would like to acknowledge Sergei Gasilov for technical support at the BMIT beamline and image reconstruction tools for CT data. The authors acknowledge the financial assistance of the Natural Sciences and Engineering Research Council of Canada.

## Appendix A Supplementary data

Supplementary data to this article can be found online at <https://doi.org/10.1016/j.crfs.2025.101002>.

## Data availability

Data will be made available on request.

## References

- Chen, J., Ghazani, S.M., Stobbs, J.A., et al., 2021. Tempering of cocoa butter and chocolate using minor lipidic components. *Nat. Commun.* 12, 5018. <https://doi.org/10.1038/s41467-021-25206-1>.
- Contessi Negrini, N., Toffoletto, N., Farè, S., Altomare, L., 2020. Plant tissues as 3D natural scaffolds for adipose, bone and tendon tissue regeneration. *Front. Bioeng. Biotechnol.* 8. <https://doi.org/10.3389/fbioe.2020.00723>.
- Craig, W.J., Mangels, A.R., Brothers, C.J., 2022. Nutritional profiles of non-dairy plant-based cheese alternatives. *Nutrients* 14, 1247. <https://doi.org/10.3390/nu14061247>.
- Czapalay, E., Marangoni, A., 2024. Functional properties of oleogels and emulsion gels as adipose tissue mimetics. *Trends Food Sci. Technol.* 153, 104753. <https://doi.org/10.1016/j.tifs.2024.104753>.
- Faragó, T., Gasilov, S., Emslie, I., Zuber, M., Helfen, L., Vogelgesang, M., Baumbach, T., 2022. Tofu: a fast, versatile and user-friendly image processing toolkit for computed tomography. *J. Synchrotron Radiat.* 29 (3), 916–927. <https://doi-org.subzero.lib.uoguelph.ca/10.1107/S160057752200282X>.
- He, J., Zhao, Y., Jin, X., Zhu, X., Fang, Y., 2021. Material perspective on the structural design of artificial meat. *Adv. Sustain. Sys.* 5 (8). <https://doi.org/10.1002/adsu.202100017>. Article 2100017.
- Paganin, D., Mayo, S.C., Gureyev, T.E., Miller, P.R., Wilkins, S.W., 2002. Simultaneous phase and amplitude extraction from a single defocused image of a homogeneous object. *J. Microsc.* 206 (1), 33–40. <https://doi-org.subzero.lib.uoguelph.ca/10.1046/j.1365-2818.2002.01010.x>.
- Palomo-Vélez, G., Tybur, J.M., van Vugt, M., 2018. Unsustainable, unhealthy, or disgusting? Comparing different persuasive messages against meat consumption. *J. Environ. Psychol.* 58, 63–71. <https://doi.org/10.1016/j.jenvp.2018.08.002>.
- Poore, J., Nemecek, T., 2018. Reducing food's environmental impacts through producers and consumers. *Science* 360, 987–992. <https://doi.org/10.1126/science.aag0216>.
- Sivakumar, Chitra, Jarvis A. Stobbs, Kaiyang Tu, Chithra Karunakaran, and Jitendra Paliwal. Unravelling Particle Morphology and Flour Porosity of Roller-Milled Green Lentil Flour Using Scanning Electron Microscopy and Synchrotron X-Ray Micro-Computed Tomography. *Powder Technol.* 436, 119470. <https://doi.org/10.1016/j.powtec.2024.119470>.
- Soleimani, Y., Ghazani, S.M., Marangoni, A.G., 2023. Enzymatic glycerolysis for the conversion of plant oils into animal fat mimetics. *Food Res. Int.* 174, 113651. <https://doi.org/10.1016/j.foodres.2023.113651>.
- Soleimani, Y., Ghazani, S.M., Marangoni, A.G., 2024a. Rheological properties of ethylcellulose oleogels of oil glycerolysis products as functional adipose tissue mimetics. *Food Hydrocoll.* 151, 109868. <https://doi.org/10.1016/j.foodhyd.2024.109868>.
- Soleimani, Y., Ghazani, S.M., Marangoni, A.G., 2024b. Ethylcellulose oleogels of oil glycerolysis products as functional adipose tissue mimetics. *Food Hydrocoll.* 151. <https://doi.org/10.1016/j.foodhyd.2024.109756>.
- Stobbs, Jarvis A., Pensini, Erica, Ghazani, Saeed M., Leontowich, Adam F.G., Quirk, Amanda, Tu, Kaiyang, Prévost, Sylvain, Mahmoudi, Najet, Fameau, Anne-Laure, Marangoni, Alejandro G., 2024. Phospholipid self-assembly in cocoa butter provides a crystallizing surface for seeding the form V polymorph in chocolate. *Cryst. Growth Des.* 24 (7), 2685–2699. <https://doi.org/10.1021/acs.cgd.3c01130>.
- Vogelgesang, M., Farago, T., Morgener, T.F., Helfen, L., dos Santos Rolo, T., Myagotin, A., Baumbach, T., 2016. Real-time image-content-based beamline control for smart 4D X-ray imaging. *J. Synchrotron Radiat.* 23 (5), 1254–1263. <https://doi.org/10.1107/S1600577516010195>.
- Wijarnprecha, K., Fuhrmann, P., Gregson, C., Sillick, M., Sonwai, S., Rousseau, D., 2022a. Temperature-dependent properties of fat in adipose tissue from pork, beef and lamb. Part 2: rheology and texture. *Food Funct.* 13, 7132–7143. <https://doi.org/10.1039/D2FO00582D>.
- Wijarnprecha, K., Gregson, C., Sillick, M., Fuhrmann, P., Sonwai, S., Rousseau, D., 2022b. Temperature-dependent properties of fat in adipose tissue from pork, beef and lamb. Part 1: microstructural, thermal, and spectroscopic characterisation. *Food Funct.* 13, 7112–7122. <https://doi.org/10.1039/D2FO00581F>.
- Willick, I.R., Stobbs, J., Karunakaran, C., Tanino, K.K., 2020. Phenotyping plant cellular and tissue level responses to cold with synchrotron-based fourier-transform infrared spectroscopy and X-ray computed tomography. In: Hinch, D., Zuther, E. (Eds.), *Plant Cold Acclimation. Methods in Molecular Biology*, vol. 2156. Humana, New York, NY. [https://doi.org/10.1007/978-1-0716-0660-5\\_11](https://doi.org/10.1007/978-1-0716-0660-5_11).